[CANCER RESEARCH 63, 1999–2004, May 1, 2003]

Advances in Brief

Real-Time Vital Optical Imaging of Precancer Using Anti-Epidermal Growth Factor Receptor Antibodies Conjugated to Gold Nanoparticles[1]

Konstantin Sokolov, Michele Follen, Jesse Aaron, Ina Pavlova, Anais Malpica, Reuben Lotan, and Rebecca Richards-Kortum[2]

Departments of Imaging Physics [K. S.], Pathology [A. M.], and Thoracic Head & Neck, Medical Oncology [R. L.] and Center for Biomedical Engineering [M. F.], University of Texas M. D. Anderson Cancer Center, Houston, Texas 77030, and Department of Biomedical Engineering, University of Texas, Austin, Texas 78712 [J. A., I. P., R. R-K.]

Abstract

Recent developments in photonic technology provide the ability to noninvasively image cells *in vivo*; these new cellular imaging technologies have the potential to dramatically improve the prevention, detection, and therapy of epithelial cancers. Endoscope-compatible microscopies, such as optical coherence tomography and reflectance confocal microscopy, image reflected light, providing a three-dimensional picture of tissue microanatomy with excellent spatial resolution (1–10 μm). However, their ability to image molecular biomarkers associated with cancer is limited. Here, we describe a new class of molecular specific contrast agents for vital reflectance imaging based on gold nanoparticles attached to probe molecules with high affinity for specific cellular biomarkers. The application of gold bioconjugates for vital imaging of precancers is demonstrated using cancer cell suspensions, three-dimensional cell cultures, and normal and neoplastic fresh cervical biopsies. We show that gold conjugates can be delivered topically for imaging throughout the whole epithelium. These contrast agents have potential to extend the ability of vital reflectance microscopies for *in vivo* molecular imaging. They can potentially enable combined screening, detection, and therapy of disease using inexpensive imaging systems; such tools could allow mass screening of diseases such as cancer in resource-poor settings.

Introduction

Early diagnosis of premalignant and malignant lesions is essential for improving the current poor survival of patients with a variety of cancers. Noninvasive diagnostic methods are especially needed for the screening of large populations for the identification of high-risk individuals who can then be followed up frequently and/or enrolled in chemoprevention trials. In the past decade, a number of microscopic techniques have been developed to image living tissue with subcellular resolution. Vital microscopies, such as OCT[3] and RCM, image reflected light, providing a detailed three-dimensional picture of tissue microanatomy without the need for physical sectioning (1, 2). These technologies provide excellent spatial resolution (1–10 μm) with penetration depth ranging from 300 μm to 1–2 mm. The resulting histological quality images can identify and monitor neoplastic changes in epithelium (3, 4). Recently, endoscope-compatible fiber optic OCT and RCM systems have been developed to image tissue microanatomy *in vivo* in near real time (4, 5). These systems are portable and inexpensive compared with other high-resolution imaging technologies such as magnetic resonance imaging microscopy; as such, they are ideally suited for early screening and diagnosis of superficial disease.

Tissue reflectance is produced by refractive index mismatches; sources of contrast in OCT and RCM images include structures with increased refractive index such as mitochondria, nuclear chromatin, and melanin (2, 3). Nonspecific contrast agents, such as AA, can perturb the nuclear refractive index distribution, increasing the ability to visualize cellular anatomy (6). Whereas OCT and RCM provide images of tissue microanatomy, their ability to image molecular changes associated with carcinogenesis is limited.

In the last few years, global analysis of gene expression by genomic and proteomic approaches has led to the discovery of new cancer-related genes, proteins, and biomarkers. Currently, most of these biomolecular signatures can only be assessed through invasive, painful biopsy. The ability to noninvasively image the expression of these biomarkers could translate into improved ability to screen and detect neoplastic changes, better ability to select and monitor therapy, and new tools to understand the pathobiology of the disease.

Here, we demonstrate a new class of molecular specific contrast agents for vital optical imaging of precancers and cancers, based on gold nanoparticles conjugated to probe molecules with high affinity for cellular biomarkers. Gold nanoparticles have been used extensively as molecular specific stains in electron microscopy (7, 8). As a result, the fundamental principles of interactions between gold particles and biomolecules have been thoroughly studied. The nanoparticles also exhibit the ability to resonantly scatter visible and near infrared light. This property is the result of excitation of surface plasmon resonances and is extremely sensitive to the size, shape, and aggregation state of the particles (9). The ability to resonantly scatter visible and near infrared light has not been explored for vital microscopy in living specimens.

In this report, we describe bioconjugates of gold nanoparticles with monoclonal antibodies against EGFR, a transmembrane M_r 170,000 glycoprotein that is overexpressed in epithelial precancers (10, 11), for molecular specific optical imaging. A high level of EGFR expression is often associated with enhanced aggressiveness of epithelial cancers and poor prognosis (12, 13). In these studies, we used gold nanoparticles of ~12 nm in diameter. This size is approximately the same as the size of antibodies, which are routinely used for molecular specific labeling and targeting.

To demonstrate the application of gold bioconjugates for vital reflectance imaging, we used three biologically relevant models of cancer with increasing complexity. First, suspensions of cervical cancer cells were explored; SiHa cells are well-characterized cervical epithelial cancer cells that overexpress EGFR (11, 14). Next, engineered tissue constructs, three-dimensional cell cultures that mimic major features of epithelial tissue (15, 16), were explored. We prepared engineered tissue constructs consisting of densely packed, multiple layers of SiHa cells atop a collagen stroma. Finally, we demonstrated the application of contrast agents in normal and neoplastic

Received 10/21/02; accepted 3/18/03.

The costs of publication of this article were defrayed in part by the payment of page charges. This article must therefore be hereby marked *advertisement* in accordance with 18 U.S.C. Section 1734 solely to indicate this fact.

[1] Supported by NSF Grant BES-0119450.

[2] To whom requests for reprints should be addressed, at Department of Biomedical Engineering, ENS 8, University of Texas, Austin, TX 78712. Phone: (512) 471-2104; Fax: (512) 475-8854; E-mail: kortum@mail.utexas.edu.

[3] The abbreviations used are: OCT, optical coherence tomography; RCM, reflectance confocal microscopy; EGFR, epidermal growth factor receptor; PVP, polyvinyl pyrrolidone; FDA, Food and Drug Administration; AA, acetic acid.

fresh cervical biopsies, the model system that most closely resembles living human epithelial tissue (17).

Materials and Methods

Preparation of Gold Bioconjugates. Colloidal gold of various sizes was prepared using citrate reduction of chloroauric acid ($HAuCl_4$) according to the method described in Ref. 18. To prepare conjugates, colloidal gold was diluted twice in 20 mM HEPES buffer (pH 7.4), and anti-EGFR monoclonal antibodies (host mouse; Sigma) were reconstituted in the same buffer at 100 μg/ml. Then the solutions were mixed at a 1:1 volume ratio and allowed to interact for 20 min at room temperature. Polyethyleneglycol (M_r 20,000; Sigma) was added to the mixture up to a final concentration of 0.2 mg/ml, and the solution was centrifuged twice at 5000 rpm for 2 h to wash unbound antibodies. After the second wash, the pellet was resuspended in PBS.

Preparation of Cells. SiHa cells were grown inside tissue culture flasks covered with collagen type I (Roche) in DMEM plus 5% FBS at 37°C under 5% CO_2. Cells were harvested using 1 mg/ml collagenase (Roche) in PBS at 37°C for ~20 min, or until the collagen substrate was entirely disassociated, and washed in DMEM. The cell suspension was labeled with gold conjugate at room temperature for ~30 min on a shaker to prevent sedimentation. The labeled cells were placed on top of a microscope slide coated with gelatin to eliminate background scattering from the glass substrate during reflectance imaging.

Preparation of Epithelial Tissue Constructs. To prepare the constructs, a suspension of epithelial cells was spun down, and a very small amount of buffered collagen type I solution (3 mg/ml) was added to the pellet. The mixture was transferred to 6.5-mm ELISA plate wells and allowed to gel at 37°C for 20 min. The volume of the mixture was adjusted to form gels with a thickness between 400 and 600 μm. The gel with embedded cells was kept in DMEM plus 5% FBS for 24–48 h. During this time, the cells continued to grow, resulting in formation of a highly dense structure consisting of multiple layers of epithelial cells. The contrast agents were added on top of the tissue phantoms in 10% PVP solution in PBS or in pure PBS. After incubation for ~30 min at room temperature, the phantoms were transversely sectioned with a Krumdieck tissue slicer, and the sections were imaged using Zeiss Leica inverted laser scanning confocal microscope.

Preparation of Fresh Cervical Biopsies. Colposcopically normal and abnormal cervical biopsies were obtained, with written consent, from women seen in the University of Texas M. D. Anderson Cancer Center Colposcopy Clinic. Biopsies were immediately placed in chilled (4°C) culture medium (DMEM without phenol red) and then embedded in 4% agarose. Subsequently, a Krumdieck tissue slicer was used to obtain transverse, 200-μm-thick fresh tissue slices. The slices were placed in a PBS solution of anti-EGFR/gold conjugates for ~30 min at room temperature. After incubation with contrast agents, the sections were washed in PBS and imaged. After imaging, the sections were subjected to H&E staining and histopathological analysis.

The wavelength dependence of light scattering was measured using the optical set-up described in Ref. 19. Briefly, samples were illuminated by a broad-band light source (halogen lamp; Dolan-Jenner Industries), and the scattered light was focused on the 250-μm entrance slit of a single grating spectrograph (F/3.8; 300 lines/mm grating; Monospec 18; Jarrel Ash) coupled to an intensified photodiode array detector (IRY-700; Princeton Instruments). Spectra were normalized by scattering from a "white" diffusely scattering substrate (Labsphere) to account for the wavelength dependence of the light source and the spectrometer.

Confocal Microscopy. The series of through focus confocal images were acquired using Zeiss Leica inverted epifluorescence/reflectance laser scanning confocal microscope with a ×40 oil immersion objective or a ×10 objective. The excitation was provided by a Kr/Ar mixed gas laser.

Results and Discussion

The scattering cross-section of gold nanoparticles is extremely high compared with polymeric spheres of the same size (Fig. 1), especially in the red region of the spectrum. This property is crucial for development of contrast agents for optical imaging in living organisms because light penetration depth in tissue dramatically increases with increasing wavelength. Another interesting optical property of gold

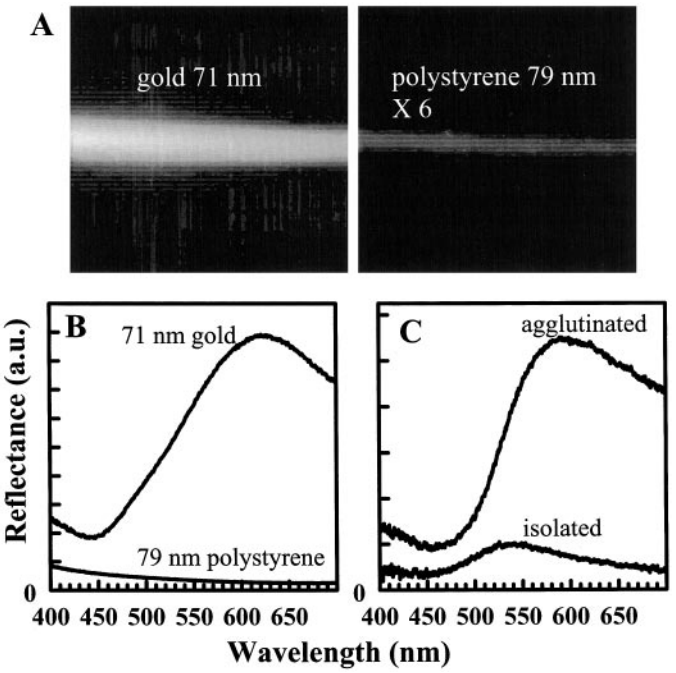

Fig. 1. Scattering properties of gold nanoparticles. *A* and *B* compare scattering of gold particles and polystyrene beads of approximately the same diameter. In *A*, suspensions of gold particles (*left*) and the polymeric spheres (*right*) were illuminated by a laser pointer that provides light in the 630–680 nm region. The images were obtained using a regular web camera at a 90° angle relative to illumination. To acquire the images of both suspensions under the same conditions, the concentration of the polymeric beads (in particles/ml) was increased 6-fold relative to the concentration of the metal nanoparticles. *B* shows the wavelength dependence of visible light scattering by the polystyrene spheres and the gold nanoparticles. The spectra were obtained from suspensions with the same concentration of metal and polymeric nanospheres. *C* compares scattering of isolated and closely spaced (agglutinated) conjugates of 12-nm gold nanoparticles with monoclonal antibodies for EGFR. Polyclonal antibodies specific for mouse IgG (Sigma) were added to induce agglutination of the conjugates.

nanoparticles that can be exploited for vital optical imaging is the increase in scattering cross-section per particle when the particles agglutinate (Fig. 1*C*). These changes produce a large optical contrast between isolated gold particles and assemblies of gold particles. This increase in contrast improves the ability to image markers that are not uniquely expressed in diseased tissue but are expressed at higher levels relative to normal tissue (such as EGFR) and to develop highly sensitive labeling procedures that do not require intermediate washing steps to remove single unbound particles.

The preparation of gold bioconjugates is based on noncovalent binding of the anti-EGFR IgG antibodies at their isoelectric point (point of zero net charge of the protein) to gold particles. The complex formation is irreversible and very stable. Specific optical changes in UV-visible spectrum of gold nanoparticles indicate binding of the antibodies: a characteristic red shift (~6 nm) of the maximum of the surface plasmon resonance and ~10% decrease in transmission. These optical changes are associated with alterations in the local refractive index around the particles after binding of the monoclonal antibodies. An additional indication of protein binding to the surface of the nanoparticles is their stability in PBS. The gold conjugates are monodispersed in the saline solution, whereas a suspension with "bare" gold particles quickly changes its color from red to blue upon addition of the saline as a result of aggregation of the nanoparticles. The anti-EGFR/gold complexes also undergo molecular specific agglutination when anti-IgG polyclonal antibodies are added to the suspension of the conjugates. The agglutination results in increased scattering by the conjugates (Fig. 1*C*).

Fig. 2, *A*–*D*, shows confocal reflectance images and combined

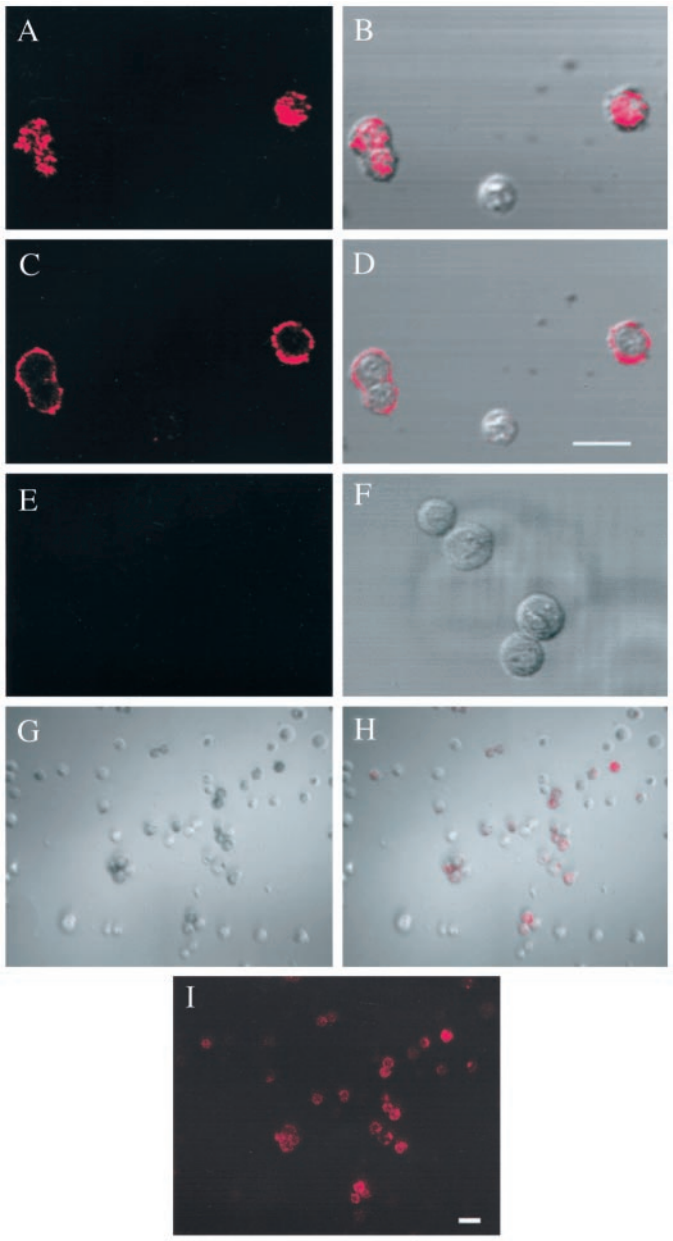

Fig. 2. High ($A-D$)- and low ($G-I$)-resolution optical images of SiHa cells labeled with anti-EGFR/gold conjugates. Nonspecific labeling using gold conjugates with BSA is shown in *E* and *F*. Laser scanning confocal reflectance (*A, C,* and *E*) and combined confocal reflectance/transmittance (*B, D,* and *F*) images of the labeled SiHa cells were obtained with ×40 objective. The scattering from gold conjugates is false-colored in *red*. In *A* and *B*, the focal plane is at the top of the cells. In *C* and *D*, the middle cross-section of the cells is in focus. The confocal reflectance and transmittance images were obtained independently and then overlaid. Reflectance images were obtained with 647 nm laser excitation. The *scale bar* is ~20 μm ($A-F$). $G-I$, a series of bright-field and reflectance images of the labeled SiHa cells obtained with ×20 objective using a combination of white light and laser pointer illumination. *G*, white light illumination; *H*, white light with laser pointer illumination at grazing incidence; *I*, laser pointer illumination at grazing incidence. The scattering of gold conjugates is false-colored in *red*. The laser pointer emits light in the 630–680 nm region with power output < 5 mW. The laser pointer illuminated an area ~3–5 mm in diameter. The *scale bar* is ~30 μm.

transmittance/reflectance images of SiHa cells labeled with anti-EGFR/gold conjugates. In a series of through focus confocal reflectance images of labeled cells, the bound conjugates first appear as randomly distributed bright spots at the top of the cells, and then bright rings can be seen in the optical cross-sections through the middle of the cells. Comparison of the labeling pattern with transmittance images of the cells indicates that labeling predominately occurs on the surface of the cellular cytoplasmic membrane. The labeling pattern is consistent with the fact that the monoclonal antibodies have molecular specificity to the extracellular domain of EGFR. The intensity of light scattering from the labeled SiHa cells is ~50 times higher than that from unlabeled cells. Therefore, unlabeled cells cannot be resolved on the dark background. No labeling was observed when gold conjugates with BSA were added to the cells (Fig. 2, *E* and *F*).

We conducted reflectance imaging before and after the unbound gold conjugates were washed from the cell suspension. The unbound gold particles were not visible before or after washing. UV-visible measurements of a washed suspension of labeled cells showed an increase in extinction of the nanoparticles in the red optical region. This change is characteristic for agglutination of the nanoparticles and indicates that the particles form closely spaced assemblies on the surface of the cells. We demonstrated that agglutination of anti-EGFR gold conjugates results in increase of scattering of particles forming the assembly (Fig. 1*C*). We believe that similar effect can contribute to the contrast between the labeled cells and the isolated, unbound conjugates.

Using UV-visible spectroscopy, we estimated the average amount of gold conjugates bound/cell (data not shown). Scattering from cells, their relatively quick sedimentation, and changes of optical properties of the particles upon binding make it difficult to measure the amount of bound nanoparticles directly. Instead, we centrifuged the labeled cells and measured the decrease in absorbance of the supernatant relative to the original suspension of the conjugates. Using this approach, we calculated that approximately 5×10^4 conjugates are bound per cell. Our results correlate well with previously published studies, which report that most cell types express from 2×10^4 to 20×10^4 EGFRs/cell (10).

We observed heterogeneous labeling of SiHa cells in suspension. To ensure that preparation of cell suspensions did not affect the extracellular domain of EGFR and produce heterogeneous labeling, we grew cells on collagen and used collagenase to harvest the cells. The same heterogeneity was also observed when the cells were labeled directly on the surface of the collagen matrix without harvesting. Heterogeneity of protein expression in cell lines is not uncommon and has been described previously in the case of EGFR (20).

The light scattering from the labeled cells is so strong that it can be easily observed using low-magnification optics and an inexpensive light source such as a laser pointer. Fig. 2, $G-I$, shows a series of images of labeled SiHa cells placed on a microscope slide obtained using a ×20 objective. In bright-field transmission, the cells with bound gold conjugates appear darker due to light absorption by the metal nanoparticles in the green optical region, and the unlabeled cells appear more transparent (Fig. 2*G*). When the sample is illuminated by a laser pointer at grazing incidence, the labeled cells appear bright due to scattered light (Fig. 2*H*). Finally, after bright-field illumination is turned off, only labeled cells can be seen (Fig. 2*I*). No scattering was observed when cells labeled using gold conjugates with BSA were illuminated by a laser pointer under the same conditions.

Bright "honey-comb"-like structures can be seen in laser scanning confocal reflectance images of abnormal cervical biopsies labeled with anti-EGFR/gold complexes (Fig. 3*A*). Scattering from the labeled cytoplasmic membranes of epithelial cells forms this pattern. No labeling of the normal biopsy can be seen when the sample is imaged under the same acquisition conditions as the abnormal sample (Fig. 3*C*). The morphology of the normal biopsy can be resolved after addition of a nonspecific contrast agent (AA) and increasing the laser power by ~6-fold (Fig. 3*E*). AA enhances fluctuations in the nuclear refractive index related to chromatin texture, enhancing scattering from nuclei (6). An increase in scattering of stroma is also evident

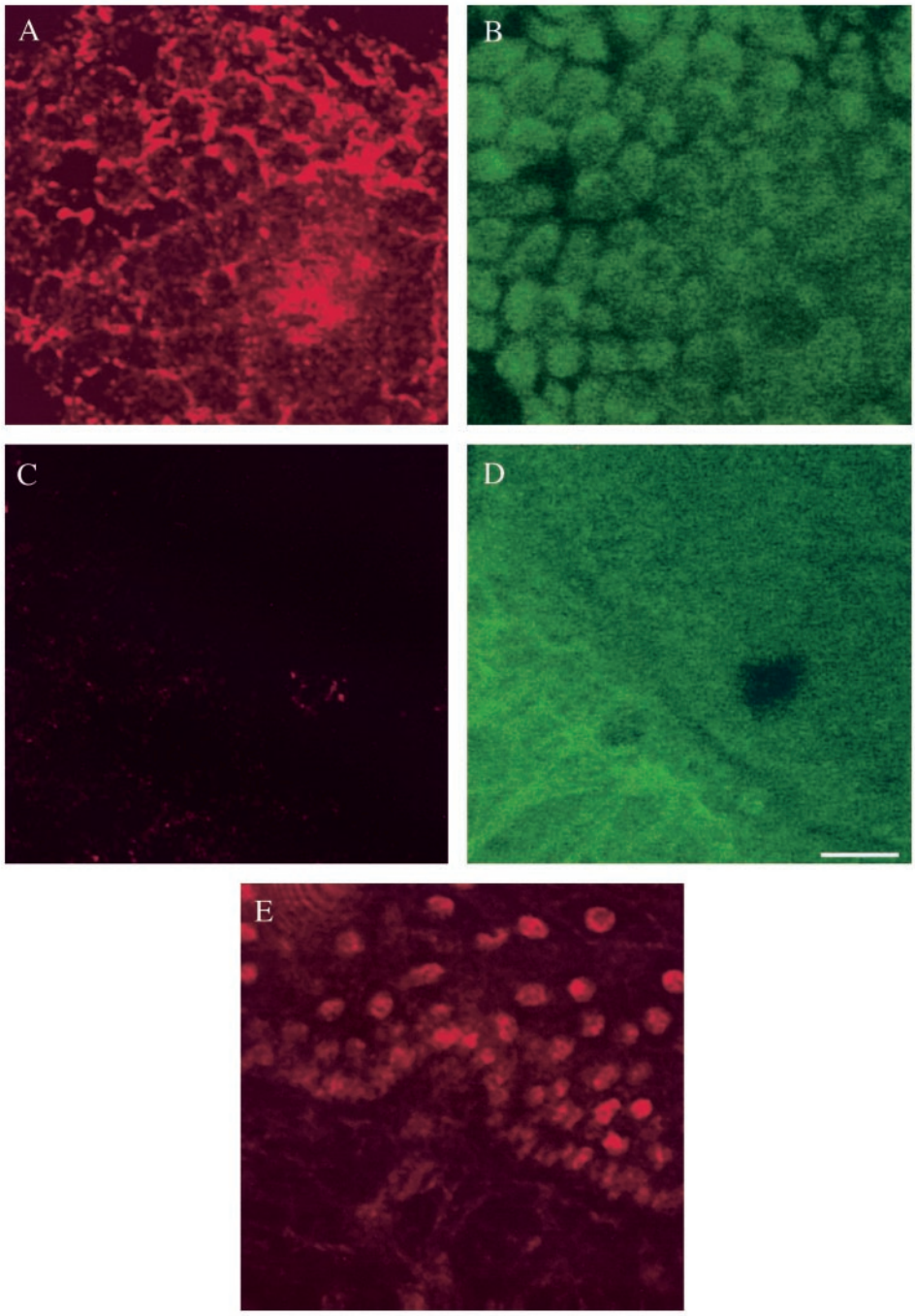

Fig. 3. Laser scanning confocal reflectance (*A*, *C*, and *E*) and confocal fluorescence (*B* and *D*) images of precancerous (*A* and *B*) and normal (*C*−*E*) fresh cervical *ex vivo* tissue labeled with anti-EGFR/gold conjugates. Reflectance images were obtained with 647 nm excitation wavelength, and fluorescence images were obtained using 488 nm excitation and 515 nm long band-pass emission filter. Reflectance images *A* and *C* were obtained after labeling with gold conjugates under the same acquisition conditions. Image *E* was obtained after 6% AA solution was added to the normal cervical biopsy and laser power was increased by ~6-fold. AA is a nonspecific contrast agent that is used in reflectance imaging of epithelium to increase scattering from nuclei (6). Confocal fluorescence images *B* and *D* were obtained under the same acquisition conditions. The reflectance images are false-colored in *red*. The *scale bar* is ~20 μm.

(Fig. 3*E*). There is no binding of anti-EGFR/gold conjugates to the stromal layer of cervical biopsies.

In corresponding autofluorescence confocal images obtained using 488 nm excitation, the epithelial cells exhibit cytoplasmic fluorescence (Fig. 3, *B* and *D*) due to mitochondrial flavin adenine dinucleotide (17). In the fluorescence image of the abnormal cervical biopsy, the epithelial cells appear to be surrounded by black contours (Fig. 3*B*). These contours are formed by the bound gold conjugates that strongly absorb visible light in the green optical region, where most of the autofluorescence signal is emitted (Fig. 1, *B* and *C*). The comparison of the reflectance and the fluorescence confocal images of the abnormal biopsy confirms predominant binding of the anti-EGFR/gold conjugates to the cytoplasmic membrane of the epithelial cells (Fig. 3, *A* and *B*).

Thus, the contrast agents presented here, coupled with vital reflectance microscopies, have the potential to yield both anatomical and molecular images of epithelial pathology. A particularly important potential application is the early detection of precancerous lesions. Early detection of curable precancers has the potential to dramatically reduce the incidence and mortality of cancer. However, *in vivo* application of these contrast agents depends on the ability to deliver the agents throughout the epithelium in the organ site of interest. Precancers of squamous epithelium originate at the basal layer, which can be located 300–500 μm beneath the tissue surface; therefore, to develop new diagnostic tools and to study the earliest molecular changes associated with cancer progression, it is imperative to deliver the gold nanoparticles throughout the whole epithelium. Using engineered tissue constructs, we demonstrated that penetration enhancers used for

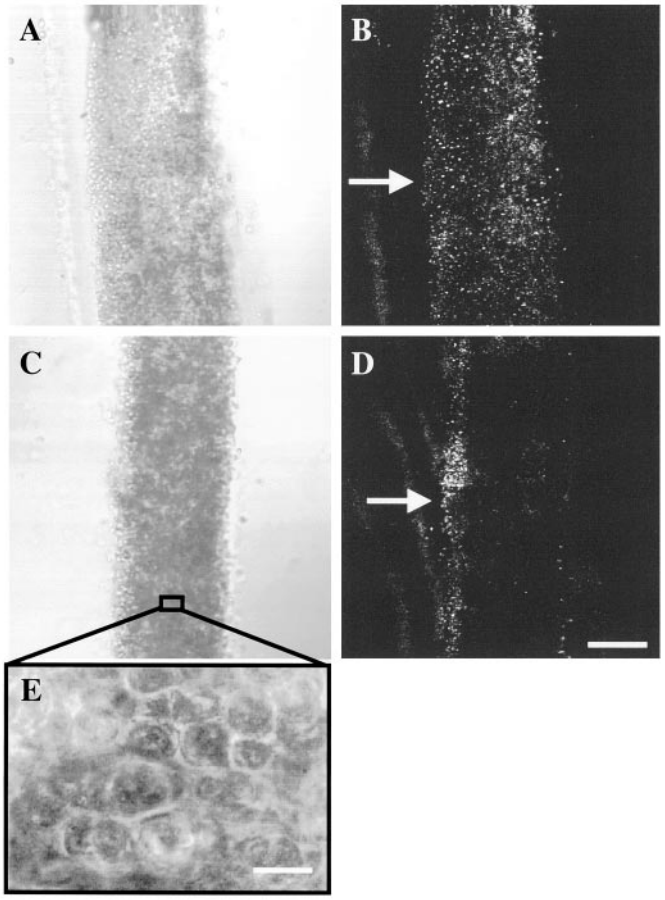

Fig. 4. Transmittance (*A*, *C*, and *E*) and reflectance (*B* and *D*) images of engineered tissue constructs labeled with anti-EGFR/gold conjugates. The tissue constructs consist of densely packed, multiple layers of cervical cancer (SiHa) cells. The contrast agents were added on top of the tissue phantoms in 10% PVP solution in PBS (*A* and *B*) or in pure PBS (*C* and *D*). After incubation for ~30 min at room temperature, the phantoms were transversely sectioned with a Krumdieck tissue slicer, and the sections were imaged using the Zeiss Leica inverted laser scanning confocal microscope with ×10 (*A*−*D*) objective. A small spot on a tissue construct was imaged using ×40 oil immersion objective to show high density of the epithelial cells in the phantom (*E*). Reflectance images were obtained with 647 nm excitation. *Arrows* show the surfaces exposed to the contrast agents. The *scale bars* are ~200 μm (*A*−*D*) and ~20 μm (*E*).

topical drug delivery, such as PVP, can be used to deliver the gold nanoparticles throughout the epithelium (Fig. 4). PVP is approved by FDA for human use as an excipient in topical formulations (*e.g.*, Povidone). The anti-EGFR/gold conjugates were applied to the top of engineered tissue constructs in pure PBS buffer and in PBS in the presence of 10% PVP. After ~30-min incubation, constructs were washed in PBS, and 200-μm-thick transverse sections were prepared and imaged using transmittance and confocal reflectance microscopies (Fig. 4). When the conjugates are applied in the presence of PVP, uniform labeling is achieved throughout the whole depth (~400 μm; Fig. 4, *A* and *B*). When gold conjugates are applied in PBS, only the surface layer of epithelial cells in the engineered tissue constructs is labeled (Fig. 4, *C* and *D*).

The contrast agents presented here indicate the tremendous potential to extend the ability of vital reflectance microscopies for *in vivo* molecular imaging. Using these contrast agents, we demonstrated the ability to image the distribution of EGFR expression in living neoplastic cervical tissue, providing the possibility to assess molecular pathology *in vivo*. Currently, the prognosis of patients with cancer is predicted mainly based on microanatomic features of disease; however, the use of molecular markers has recently shown promise to better predict patient outcomes and to select therapies (21). In the absence of contrast agents, OCT and RCM yield images of tissue microanatomy similar to that which can be obtained with conventional histopathology; contrast agents based on gold nanoparticles provide a strong source of signal with molecular specificity that is immune to photobleaching.

Other reflectance-based technologies that have been developed to image disease in deeper tissues with lower spatial resolution may also benefit from these contrast agents. Diffuse optical tomography allows noninvasive *in vivo* imaging of oxygenated and deoxygenated hemoglobin and has been explored for detection of breast cancer (22); coupling diffuse optical tomography with the contrast agents presented here may provide more sensitive detection of smaller lesions.

Many properties of contrast agents based on gold nanoparticles make them ideally suited for vital imaging and *in vivo* diagnosis. By appropriately adjusting the size of the particles, surface plasmon resonances can be selected to take advantage of regions where tissue is most transparent, depending on the degree of tissue penetration required. Using particles of different sizes conjugated to different probe molecules, multicolor labeling for many targets can be achieved (23). The enhanced scattering from closely spaced gold particles confers important advantages for *in vivo* imaging. First, the scattering from aggregates of bound particles is greatly enhanced compared with background scattering from unbound particles. Additionally, many markers are not uniquely expressed in disease but are over- or underexpressed. The scattering from closely spaced aggregates associated with overexpression can magnify the signal difference owing to moderate levels of overexpression.

Contrast agents based on gold nanoparticle antibody conjugates have the potential for *in vivo* use, with topical or systemic delivery. The inherent biocompatibility of gold implies they can be used directly *in vivo* without the need for protective layer growth. In fact, long-term treatment of rheumatoid arthritis utilizes gold (up to a cumulative dose of 1.2–1.8 g/year for up to 10 years; Ref. 24). We anticipate that $<$0.3 mg of gold would be required for diagnosis with topical delivery to the cervix. Humanized antibodies, where a mouse antibody-binding site is transferred to a human antibody gene, are much less immunogenic in humans (25), and many humanized antibodies are currently in clinical trials. Since 1997, the FDA has approved more than 10 monoclonal antibody-based drugs, including Herceptin, for metastatic breast cancer therapy (26, 27). For surface lesions located in epithelial tissue, simple FDA-approved agents, such as PVP, can be used to increase tissue permeability and deliver contrast agents topically.

References

1. Huang, D., Swanson, E. A., Lin, C. P., Schuman, J. S., Stinson, W. G., Chang, W., Hee, M. R., Flotte, T., Gregory, K., and Puliafito, C. A. Optical coherence tomography. Science (Wash. DC), *254:* 1178–1181, 1991.
2. Rajadhyaksha, M., Grossman, M., Esterowitz, D., Webb, R. H., and Anderson, R. R. *In vivo* confocal scanning laser microscopy of human skin: melanin provides strong contrast. J. Investig. Dermatol., *104:* 946–952, 1995.
3. Collier, T., Lacy, A., Malpica, A., Follen, M., and Richards-Kortum, R. Near real-time confocal microscopy of amelanotic tissue: detection of dysplasia in *ex vivo* cervical tissue. Acad Radiol., *9:* 504, 2002.
4. Tearney, G. J., Brezinski, M. E., Bouma, B. E., Boppart, S. A., Pitris, C., Southern, J. F., and Fujimoto, J. G. *In vivo* endoscopic optical biopsy with optical coherence tomography. Science (Wash. DC), *276:* 2037–2039, 1997.
5. Liang, C., Sung, K-B., Richards-Kortum, R., and Descour, M. R. Fiber confocal reflectance microscope (FCRM) for *in-vivo* imaging. Opt. Express, *9:* 821–830, 2001.
6. Drezek, R., Collier, T., Brookner, C. K., Malpica, A., Lotan, R., Richards-Kortum, R., and Follen, M. Laser scanning confocal microscopy of cervical tissue before and after application of acetic acid. Am. J. Obstet. Gynecol., *182:* 1135–1139, 2000.
7. Horisberger, M. Colloidal gold: a cytochemical marker for light and fluorescent microscopy and for transmission and scanning electron microscopy. Scanning Electron Microsc., *11:* 9–31, 1981.
8. Geoghegan, W. D., and Ackerman, G. A. Adsorption of horseradish peroxidase, ovomucoid, and anti-immunoglobulin to colloidal gold for the indirect detection of concanavalin A, wheat germ agglutinin, and goat anti-human immunoglobulin G on

cell surfaces at the electron microscope level: a new method, theory, and application. J. Histochem. Cytochem., *25:* 1187–1200, 1977.
9. Mulvaney, P. The direct measurement of forces of interaction between a colloidal particle and an oil droplet. Langmuir, *12:* 788–800, 1996.
10. Carpenter, G. Receptors for epidermal growth factor and other polypeptide mitogens. Annu. Rev. Biochem., *56:* 881–914, 1987.
11. Maruo, T., Yamasaki, M., Ladines-Llave, C. A., and Mochizuki, M. Immunohistochemical demonstration of elevated expression of epidermal growth factor receptor in the neoplastic changes of cervical squamous epithelium. Cancer (Phila.), *69:* 1182–1187, 1992.
12. Pfeifer, D., Stellwag, B., Pfeifer, A., Borlinghaus, P., and Meier, W. Clinical implications of the epidermal growth factor receptor in the squamous cell carcinoma of the uterine cervix Gynecol. Oncol., *33:* 146–150, 1989.
13. Todd, R., and Wong, D. T. W. Epidermal growth factor receptor (EGFR) biology and human oral cancer. Histol. Histopathol., *14:* 491–500, 1999.
14. Wobus, M., Kuns, R., Wolf, C., Horn, L-C., Koehler, U., Sheyn, I., Werness, B. A., and Sherman, L. S. CD44 mediates constitutive type I receptor signaling in cervical carcinoma cells. Gynecol. Oncol., *83:* 227–234, 2001.
15. Saltzman, M. W., Parkhurst, M. R., Parsons-Wingerter, P., and Zhu, W-H. Three-dimensional cell cultures mimic tissues. Ann. N. Y. Acad. Sci., *665:* 259–273, 1992.
16. Sokolov, K., Galvan, J., Myakov, A., Lacy, A., Lotan, R., and Richards-Kortum, R. Realistic three-dimensional epithelial tissue phantoms for biomedical optics. J. Biomed. Opt., *7:* 148–156, 2002.
17. Drezek, R., Brookner, C., Pavlova, I., Boiko, I., Malpica, A., Lotan, R., Follen, M., and Richards-Kortum, R. Autofluorescence microscopy of fresh cervical-tissue sections reveals alterations in tissue biochemistry with dysplasia. Photochem. Photobiol., *73:* 636–641, 2001.
18. Frens, G. Controlled nucleation for the regulation of the particle size in monodisperse gold suspensions. Nat. Phys. Sci., *241:* 20–22, 1973.
19. Sokolov, K., Drezek, R., Gossage, K., and Richards-Kortum, R. Opt. Express, *5:* 302–317, 1999.
20. Monaghan, P., Ormerod, M. G., and O'Hare, M. J. Epidermal growth factor receptors and EGF-responsiveness of the human breast-carcinoma cell line PMC42. Int. J. Cancer, *46:* 935–943, 1990.
21. Grizzle, W. E., Manne, U., Jhala, N. C., and Weiss, H. L. Molecular characterization of colorectal neoplasia in translational research. Archiv. Pathol. Lab. Med., *125:* 91–98, 2001.
22. Ntziachristos, V., and Chance, B. Probing physiology and molecular function using optical imaging: applications to breast cancer. Breast Cancer Res., *3:* 41–46, 2001.
23. Schultz, S., Smith, D., Mock, J., and Schultz, D. Single-target molecule detection with nonbleaching multicolor optical immunolabels. Proc. Natl. Acad. Sci. USA, *97:* 996–1001, 2000.
24. Abrams, M. J., and Murrer, B. A. Metal compounds in therapy and diagnosis. Science (Wash. DC), *261:* 725–730, 1993.
25. Berkower, I. The promise and pitfalls of monoclonal antibody therapeutics. Curr. Opin. Biotechnol., *7:* 622–628, 1996.
26. Holliger, P., and Bohlen, H. Engineering antibodies for the clinic. Cancer Metastasis Rev., *18:* 411–419, 1999.
27. Weiner, L. M. Monoclonal antibody therapy of cancer. Semin. Oncol., *26* (Suppl. 12)*:* 43–51, 1999.